

The Case for an LMS Camera

Tripurari Singh

Image Algorithmics, Bethesda, MD 20816, USA

Mritunjay Singh

Image Algorithmics, Irvine, CA 92620, USA

Abstract

Consumer color cameras employ sensors that do not mimic human cone spectral sensitivities, and more generally do not meet the Luther-Ives condition since the accompanying color correction substantially amplifies noise in the red channel. This begs the question: if cone spectral sensitivities yield low SNR, why has the Human Visual System so evolved?

We answer the above question by noting that since modern ISPs – and the ancient HVS – remove virtually all chrominance noise, chrominance denoising artifacts rather than the chrominance noise itself should be considered. While sensor green, blue are reasonable analogs of the human M, S cones respectively, the spectral sensitivity of red is much narrower than that of L and does not overlap much with green. An imager employing L instead of red suffers from increased red noise but is also more sensitive. This allows a high SNR $(L+M)/2$ luminance image to be reconstructed and used for denoising.

Modeling the color filter array on the human retina, with a higher density of L pixels at the expense of S pixels, further improves the red SNR without the accompanying loss of blue quality being perceptible. The resulting LMS camera outperforms conventional RGB cameras in color accuracy and luminance SNR while being competitive in chrominance quality.

Introduction

The human retina comprises of L, M, S cones [1] with the spectral sensitivities of L, M overlapping a great deal, shown in figure 1, and together covering practically the whole spectrum defining the human visual system's luminance perception. Digital cameras do not attempt to mimic the L, M, S spectral sensitivities because differencing L, M to obtain red greatly amplifies noise.

Most consumer cameras instead employ narrower R, G, B spectral sensitivities, shown in figure 2, that do not overlap much [2], and hence can be converted to an output color space, such as sRGB, without significantly amplifying noise. The use of spectral sensitivities that differs from L, M, S, or more generally, differs from any linear combination of L, M, S and thus does not satisfy the Luther-Ives condition, is the primary source of color errors.

Colorimetric cameras, mostly designed for reprographic applications such as archival work in museums, overcome the noise amplification problem by capturing the image in more than three spectral bands [3, 4, 5, 6, 7]. Variants range from monochrome sensors coupled with liquid crystal tunable filters that capture a large number of narrow bands [8, 9] to monochrome cameras with color wheels that capture a smaller number of bands but with higher resolution and SNR to imagers where the color wheel is in the light source [10] or the illuminants are multiplexed with a DLP projector [11]. Color wheel imagers with wide band filters gen-

erally have higher SNR than those with narrow bands. A popular design is the joint Munsell Color Science Laboratory and Sinar designed Color To Match camera [12] that uses only two filters but a RGB instead of a monochrome sensor.

Single shot multispectral cameras include a 6 band, 6 image sensor system comprising of two HDTV cameras [13]. Single shot single sensor cameras overlay the image sensor with a multispectral color filter array comprising more than 3 spectral bands and use multispectral demosaicking algorithms to reconstruct the severely under sampled color planes [14, 15, 16, 17, 18, 19, 20].

While single sensor multispectral cameras avoid noise amplification in the color correction step, the effect of under sampling each color plane pushes the noise into lower frequencies, since each sample must now be used by the demosaicking algorithm to reconstruct its color in a larger surrounding area. Low frequency noise - and artifacts - are visually more objectionable than high frequency, fine grained noise and artifacts. Furthermore, multispectral demosaicking is a challenging problem and results in lower demosaicked quality. So far research in single sensor multispectral cameras has not been directed towards sensitivity or noise to the best of our knowledge.

Attempts to improve the color accuracy of trichromatic systems invariably run into noise and sensitivity issues [2, 21, 22, 23]. [2] formally poses the problem of minimizing the weighted average of color error and noise, $\overline{\Delta E_{94}^*} + \alpha \overline{\sigma}^2$, where $\overline{\sigma}^2$ is the noise variance and α is the weighting factor. They note that increasing α , and thereby increasing the importance of noise makes a large change to the red filter but not to the green and blue filters, which is expected given the L, M, S spectra. [24] also studies the trade off of color accuracy with noise but in the context of materials for color filter arrays, and uses the popular SNR10 metric to quantify noise and ΔE_{2000} to quantify color error.

In this paper we introduce chrominance denoising as a factor in the color accuracy v/s noise trade off of trichromatic cameras. Chrominance denoising produces a large visual improvement, is less challenging than luminance denoising, produces less objectionable artifacts and has become ubiquitous in consumer cameras. We show that a single shot single sensor camera with L, M, S spectral sensitivities has compelling advantages over the conventional RGB Bayer design and, in doing so, explain why the Human Visual System has so evolved.

The Case for an LMS Camera

The wider spectral sensitivity of L than red amplifies noise in the color correction step, but also makes the camera more sensitive. The resulting increase in luminance SNR can be used by the chrominance denoiser to avoid averaging across feature bound-

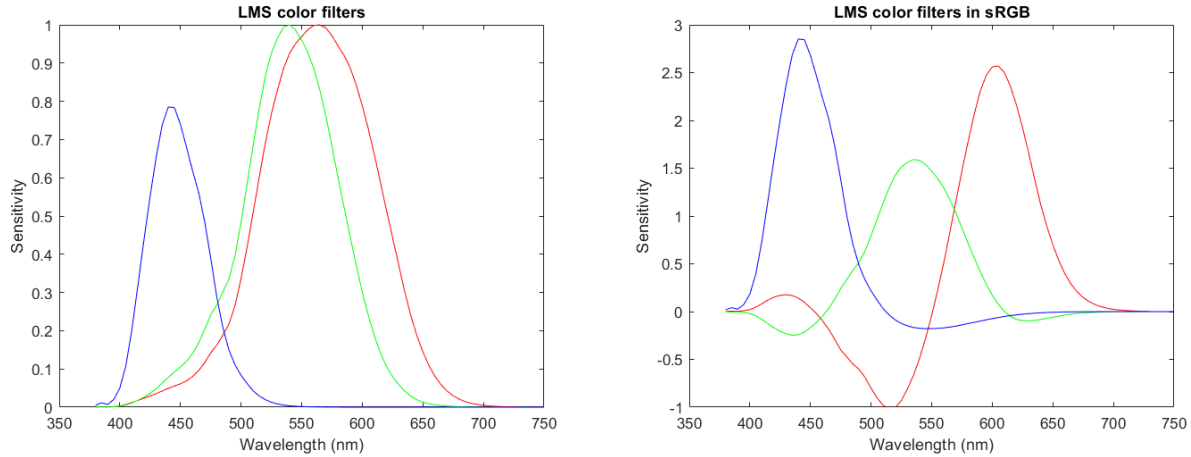


Figure 1. Sensitivity of a hypothetical LMS image sensor (left), and sensitivity after conversion to the sRGB color space (right).

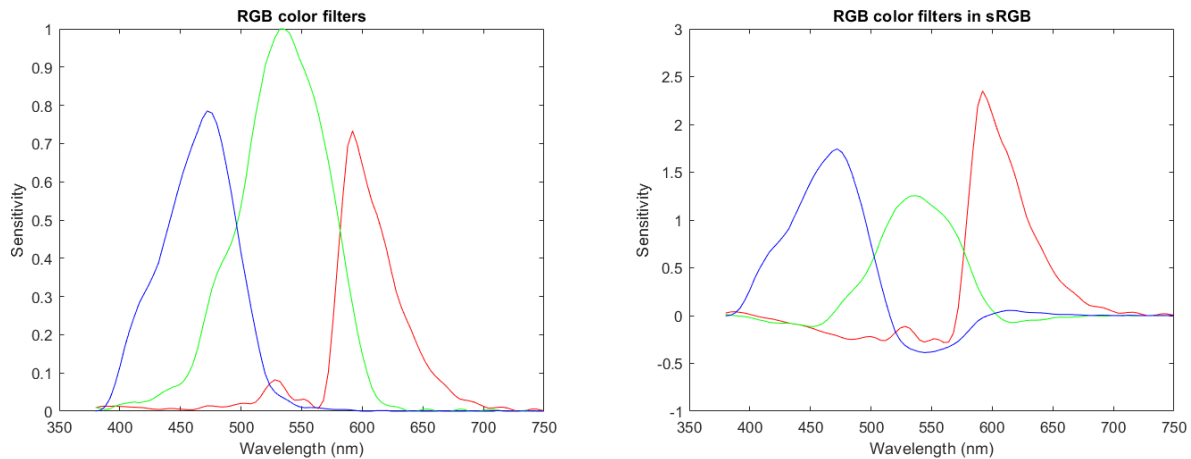


Figure 2. Sensitivity of a conventional RGB image sensor (left), and sensitivity after conversion to the sRGB color space (right).

aries and thereby decrease color bleed and color desaturation.

A camera with chrominance denoising and a Bayer sensor with LMS filters in place of RGB filters still has lower quality red than the corresponding conventional RGB Bayer camera, but the difference is greatly reduced by the chrominance denoising step. The blue, green and the luminance color planes of the LMS camera are superior to RGB, having lower noise and artifacts.

New Color Filter Array

In order to improve the red quality of the LMS camera we employ a new CFA, shown in figure 3, with double the density of L pixels and half the density of S pixels as compared to the Bayer pattern. This design is motivated by the human retina which has much higher densities of L, M cones than S cones.

To arrive at the LMS CFA pattern we first partition the square lattice of the image sensor into two quincunx lattices and assign one quincunx to L and the other to M. Next we substitute 1 in 4 M pixels with S so as to form a regular, 45 degree rotated lattice occupying 1 in 8 pixels. We substitute S pixels for M instead of L for the following reasons:

1. L is roughly 18% brighter than M on gray features in D65 lighting, hence a higher density of L pixels improves luminance SNR more than a higher density of M pixels
2. L pixels are slightly more important than M for red quality which is under stress
3. S pixels are more strongly correlated to M pixels than L allowing the demosaicker to extract more information from S pixels for the reconstruction of M than it can do for L

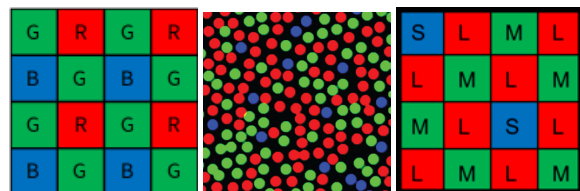


Figure 3. The Bayer CFA (left), the human retina (center), the proposed LMS CFA (right).

Doubling the density of L pixels brings red SNR and denoising artifacts roughly on par with RGB Bayer cameras. Green quality is mostly unchanged between Bayer and the proposed CFA. Blue quality is degraded by the halving of S pixel density, but blue can be denoised more aggressively than red and green since it does not contribute much to the perceived luminance [1]. The loss of S quality also has little impact on red and green quality in the color correction step owing to low importance of S in the correction of red and green. This makes the demosaicking of the proposed CFA less challenging than multispectral CFAs that have to contend with sparse samples for reconstructing red and green, in addition to blue.

Processing the Raw LMS Data

The novel LMS CFA requires a new demosaicking algorithm and also modifications to chrominance denoising to better leverage the different noise levels and noise spectra of its color planes.

Demosaicking

Demosaicking of L, M are straightforward owing to their high densities in the proposed CFA. Universal demosaickers [25, 26, 27, 28, 29] can be used as can frequency domain algorithms [30].

The spectrum of the LMS mosaicked image is shown in figure 4. While the LMS mosaic has copies of the chrominance $C2 = M - S$ overlapping with luminance in the mid frequencies with carriers at $(\pm \frac{\pi}{2}, \pm \frac{\pi}{2})$, it also has copies of the same chrominance at $(0, \pm \pi)$ and $(\pm \pi, 0)$. [25, 26], in particular, are good at removing the effects of S since they can disregard the spectral overlap of the chrominance and luminance signals if at least one copy of the chrominance does not overlap with the luminance. An algorithm based on [25, 26] is used for the experimental work described in this paper.

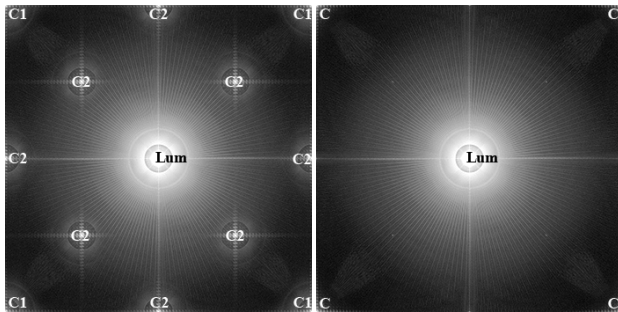


Figure 4. Spectrum of the proposed LMS CFA (left). Here $Lum=4L+3M+S$, $C1=4L-3M-S$, $C2=M-S$. Spectrum after reconstructing M at S locations (right). Here $Lum=L+M$ and $C=L-M$.

Also possible is a hybrid spatial/frequency domain algorithm that first reconstructs M at S locations using a directional average, to avoid averaging across edges, followed by a filtering operation to separate the luminance from the L-M chrominance modulated at $(\pm \pi, \pm \pi)$ (see figure 4). Next the L-M chrominance is demodulated back to baseband and L, M are recovered via linear combinations of luminance and chrominance signals thus obtained. This hybrid algorithm is given in figure 5.

Demosaicking of S requires sparse demosaicking techniques

at each S pixel location
sense edge orientation
 $M \leftarrow \text{average}(M)$ along edge direction
to obtain the LM_{mosaic}
at all pixel locations
 $luminance \leftarrow \text{LowPassFilter}(LM_{mosaic})$ reconstructed above
 $chrominance \leftarrow \text{Demodulate}(LM_{mosaic} - luminance)$
at M pixel locations
 $L \leftarrow (luminance + chrominance)/2$
at L pixel locations
 $M \leftarrow (luminance - chrominance)/2$

Figure 5. Hybrid L, M demosaicking algorithm.

such as those developed for RGBW and multispectral CFAs. One popular algorithm is to construct a guide image, such as $(L+M)/2$ and use a Joint Bilateral [31] or a Guided Image Filter [32] to reconstruct S.

Chrominance Denoising

We convert from LMS to the sRGB color space using the following equation [33],

$$\begin{bmatrix} R \\ G \\ B \end{bmatrix} = \begin{bmatrix} 4.73 & -3.87 & 0.14 \\ -0.60 & 1.75 & -0.16 \\ 0.07 & -0.26 & 1.12 \end{bmatrix} \cdot \begin{bmatrix} L \\ M \\ S \end{bmatrix} \quad (1)$$

perform chrominance denoising in the following color space,

$$\begin{aligned} luminance &= \frac{L+M}{2} \\ chrominance1 &= R - luminance \\ chrominance2 &= G - luminance \\ chrominance3 &= B - luminance \end{aligned}$$

followed by conversion back to the sRGB color space.

Denoising in the above color space brings up the quality of R, G, B color planes roughly to that of the high SNR $(L+M)/2$ color plane. It also allows us to apply different denoising strengths to each of the chrominance channels, which is important given the vastly different noise levels and noise spectra of R, G, and B. We use a multi-resolution denoiser similar to [34], but simpler bilateral or sigma filters can also be used in well lit applications.

White Balance

Most RGB Image Signal Processors (ISP) perform white balance in the sensor RGB space before demosaicking. This works well since sensor RGB spectral sensitivities are typically narrow.

LMS, with its wider L spectral sensitivity requires two rounds of white balance. The first white balance before demosaicking helps improve demosaicking performance by equalizing LMS color channel strengths. The second white balance after sharpening of spectral sensitivities helps with color constancy [35, 2]. More sophisticated color constancy algorithms can also be employed in a LMS camera.

Experimental Results

We compare images from the LMS and Bayer pipelines under a range of simulated noise levels. We measure the deviation

of the noisy images output by the processing pipelines with the clean ground truth images and report the PSNR. We also measure the SNR on gray panels of the Macbeth chart.

We do not measure color error since it is expected to be zero for LMS under our ideal simulation conditions. Nor is the measurement of Bayer color error interesting as it is already known for most cameras.

Both the LMS and Bayer pipelines consist of demosaicking, conversion to sRGB color space, chrominance denoising and application of the sRGB tone map. For LMS we employ a demosaicker based on [25, 26]. For Bayer, we employ the DLMMSE [36] algorithm that is popular with open source raw converters especially for noisy images. For chrominance denoising, we employ a multiresolution denoiser for both LMS and Bayer, with the Bayer chrominance denoiser operating in the YUV color space. No luminance denoising, or other post processing, is performed. Raw LMS and Bayer data is generated in two ways - starting from a hyperspectral image set or from a sRGB image set.

Hyperspectral Image Set

We use isetcam [37] to generate LMS images from hyperspectral image cubes with the D65 illuminant. We use the images show in figure 6. Next, we simulate diffraction limited optics with an airy disc diameter of 2 pixels. We then add noise according to the noise model of a typical 1μ pixel pitch CMOS image sensor with $1.5 e^-$ read noise and $0.14 \text{ counts}/e^-$ conversion gain, where counts is the output of a 10 bit ADC. We simulate analog gains of 4, 8, 16, 32 and 64 and also the noiseless case. Finally, we mosaic the image according to the LMS CFA pattern.

We generate the Bayer raw data in a similar manner by using the quantum efficiency of Nikon D100 instead of the LMS spectral sensitivities.

Repurposing RGB Images

The hyperspectral image sets we have access to are limited in scope and do not include several popular test targets used to test demosaicking and chrominance denoising performance. Since the superior color accuracy of an LMS camera is not in doubt and noise is the primary concern, we approximately convert RGB images of test targets to LMS with the understanding that color accuracy of the LMS images so obtained will be no different than RGB. We use the popular Kodak and IMAX image sets as well as the test charts shown in in figure 7.

To convert sRGB to LMS we reverse the usual sequence of color processing steps of an ISP - white balancing of the sensor raw data, conversion to sRGB color space and sRGB tone mapping. After linearizing the sRGB image, we apply the inverse of the color conversion matrix of equation 1. To reverse the white balance step we use the inverse of the white balance coefficients, $[1.0000, 1.2191, 3.1397]$, needed to balance the isetcam's hyperspectral Macbeth Color Chart illuminated by a D65 light source and captured with LMS spectral sensitivities. We then simulate optics, add noise and mosaic the images exactly as in the hyperspectral image set case.

We generate the Bayer raw data in a similar manner by inverting the following color conversion matrix of a typical Bayer sensor to the sRGB color space,

$$\begin{bmatrix} 1.81 & -0.53 & -0.28 \\ -0.30 & 1.38 & -0.08 \\ -0.13 & -0.33 & 1.46 \end{bmatrix}$$

and inverting the $[1.8123, 1.0000, 1.8799]$ white balance coefficients.

Results

Table 2 shows approximately 5 dB SNR lead of LMS over Bayer on the Macbeth gray panels in low light, read noise limited conditions and approximately 3.5 dB in bright light, shot noise limited conditions. The slight PSNR advantage of LMS over Bayer indicates the absence of serious artifacts, which we also visually confirm. Note that our Bayer PSNR values are higher than those previously reported because we simulate the effect of optics.

We also subjectively demonstrate good resolution and lack of false color with the Circular Zone plate, the "Siemens Star" of figure 8 and good color saturation in the presence of noise with the "Dead Leaves" of figure 9. Both the Siemens Star and the Dead Leaves crops were taken from the industry standard TE42 chart.

Fabrication of Color Filters

The LMS spectral responses are Gaussian [38] making LMS color filters easy to fabricate. For high color accuracy, the quantum efficiency of the image sensor should be taken into account so that the product of filter spectral sensitivities and quantum efficiency closely matches LMS spectral sensitivity, or a linear combination thereof (Luther-Ives condition).

Meeting the more general Luther-Ives condition instead of matching the LMS spectral sensitivities can be considered if the quantum efficiency of the sensor makes the required LMS filter spectral sensitivities deviate significantly from Gaussian functions making them hard to fabricate.

Conclusion and Future Work

This paper provides a proof of concept for an LMS camera that is:

1. colorimetric with easy to realize color filters
2. has roughly 5 dB luminance SNR advantage in low light read noise limited settings and roughly 3.5 dB in bright light shot noise limited settings over a comparable Bayer camera.
3. has roughly comparable chrominance denoising artifacts as RGB Bayer and a slight PSNR lead.

This paper focuses on the popular single sensor camera architecture, but the chrominance denoising techniques can be equally well applied to 3 sensor, beam splitter cameras, scanners and other trichromatic image capture devices.

The performance of the LMS camera is likely to improve rapidly, as is the case with most new technologies. Furthermore, the availability of LMS cameras will hopefully lead to the adoption of more sophisticated color science in image capture pipelines.

Lastly, the luminance SNR improvement over RGB sensors helps explain why the Human Visual System has so evolved.



Figure 6. The hyperspectral images from isetcam used in our experiments.

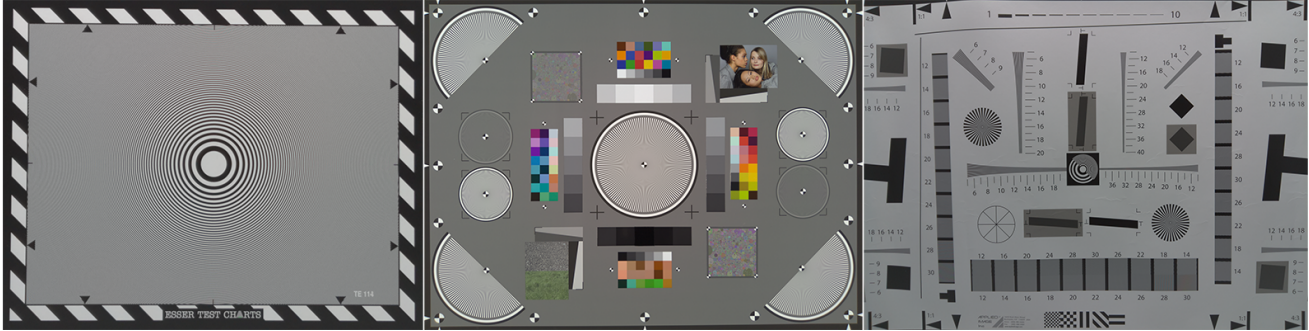


Figure 7. RGB sourced charts used in our experiments. We also test on the Kodak and IMAX image sets.

Image Set	No added noise		4x Gain		8x Gain		16x Gain		32x Gain		64x Gain	
	Bayer	LMS	Bayer	LMS	Bayer	LMS	Bayer	LMS	Bayer	LMS	Bayer	LMS
ISET (Hyperspectral)	47.10	48.93	39.02	41.23	37.48	39.44	35.03	37.28	32.86	35.26	31.20	33.55
Charts (RGB)	47.67	47.50	36.94	39.01	35.26	37.16	33.03	34.97	31.32	33.13	30.14	31.78
Kodak (RGB)	42.79	43.15	37.89	38.83	36.57	37.51	34.52	35.78	32.57	33.99	31.07	32.50
IMAX (RGB)	37.26	39.31	34.96	36.15	34.11	34.86	32.57	33.39	31.09	31.96	30.00	30.87

Table 1: PSNR, in dB, after demosaicking, conversion to sRGB color space and chrominance denoising. Note that our Bayer PSNR values are higher than those previously reported because we simulate the effect of optics.

Noise	Panel 1		Panel 2		Panel 3		Panel 4		Panel 5		Panel 6	
	Bayer	LMS										
4x Gain	17.08	21.50	21.72	25.89	24.83	28.67	27.34	31.62	29.30	33.81	31.13	34.87
8x Gain	13.90	18.44	18.61	22.79	21.82	25.84	24.32	28.82	26.36	30.99	28.14	31.84
16x Gain	11.81	15.98	16.59	20.25	19.82	23.31	22.34	26.14	24.34	28.28	26.11	29.57
32x Gain	8.59	13.07	13.60	17.45	16.91	20.51	19.45	23.34	21.46	25.44	23.21	26.79
64x Gain	1.47	7.04	7.58	12.30	11.41	15.46	14.02	18.33	16.07	20.43	17.76	21.64

Table 2: SNR, in dB, of the Mather Chart gray panels after demosaicking, conversion to sRGB color space and chrominance denoising. Left to right in the increasing order of panel brightness.

References

- [1] Stockman, A. and Sharpe, L. T., "The spectral sensitivities of the middle-and long-wavelength-sensitive cones derived from measurements in observers of known genotype," *Vision research* **40**(13), 1711–1737 (2000).
- [2] Kuniba, H. and Berns, R. S., "Spectral sensitivity optimization of color image sensors considering photon shot noise," *Journal of Electronic Imaging* **18**(2), 023002–023002 (2009).
- [3] Martinez, K., Cupitt, J., Saunders, D., and Pillay, R., "Ten years of art imaging research," *Proceedings of the IEEE* **90**(1), 28–41 (2002).
- [4] Berns, R. S., "Color-accurate image archives using spectral imaging," *Scientific Examination of Art: Modern Techniques in Conservation and Analysis* **12**, 105–119 (2005).
- [5] Fischer, C. and Kakoulli, I., "Multispectral and hyperspectral imaging technologies in conservation: current research and potential applications," *Studies in Conservation* **51**(sup1), 3–16 (2006).
- [6] Liang, H., "Advances in multispectral and hyperspectral imaging for archaeology and art conservation," *Applied Physics A* **106**, 309–323 (2012).
- [7] Habel, R., Kudenov, M., and Wimmer, M., "Practical spectral photography," in [*Computer graphics forum*], **31**(2pt2), 449–458, Wiley Online Library (2012).
- [8] Hardeberg, J. Y., Schmitt, F., and Brettel, H., "Multispectral color image capture using a liquid crystal tunable filter," *Optical engi-*

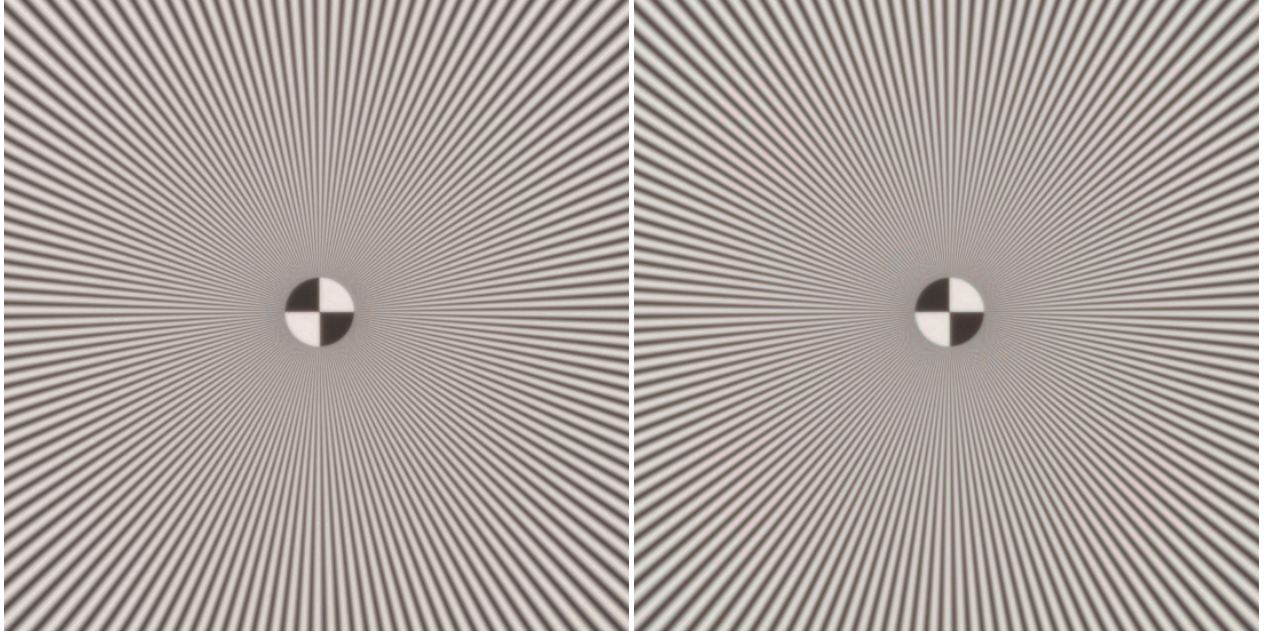


Figure 8. “Siemens Star” crop of the TE43 chart in bright light demonstrates good resolution and no visible false color. Bayer (left), LMS (right).

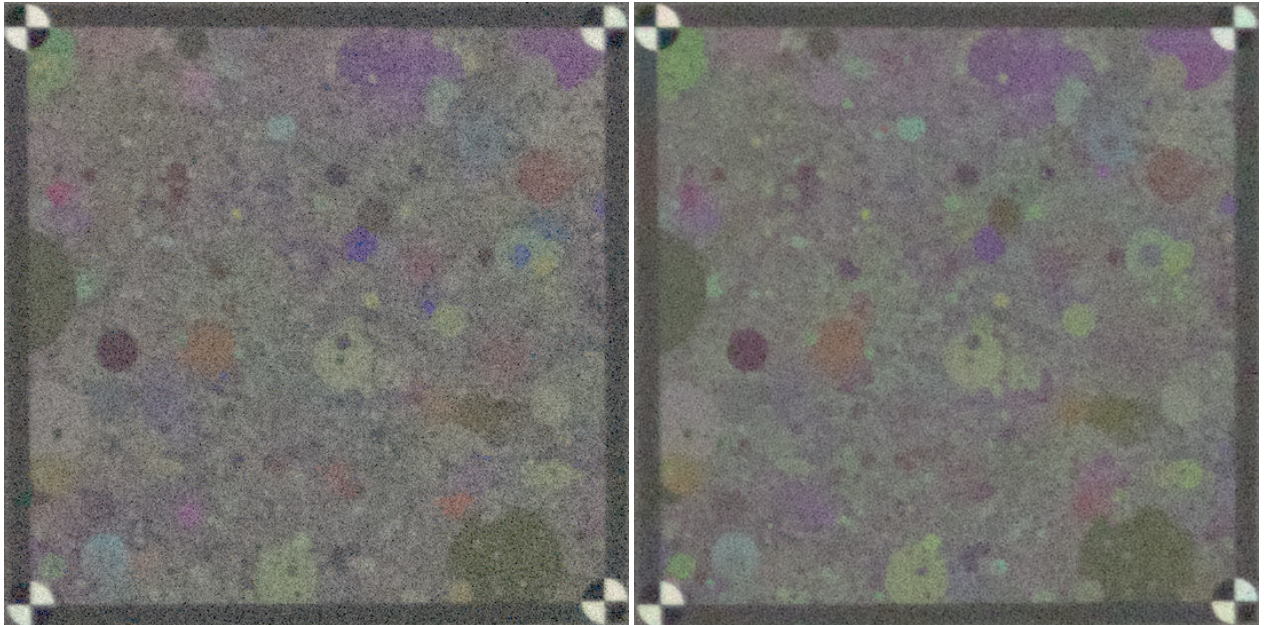


Figure 9. “Dead Leaves” crop of the TE43 chart in low light demonstrates color saturation after chrominance denoising. Bayer (left), LMS (right). Note the higher luminance SNR of LMS.

neering **41**(10), 2532–2548 (2002).

- [9] Burns, P., “Analysis of image noise in multispectral color acquisition,” (1997).
- [10] Park, J.-I., Lee, M.-H., Grossberg, M. D., and Nayar, S. K., “Multispectral imaging using multiplexed illumination,” in *[2007 IEEE 11th International Conference on Computer Vision]*, 1–8, IEEE (2007).
- [11] Han, S., Sato, I., Okabe, T., and Sato, Y., “Fast spectral reflectance

recovery using dlp projector,” *International journal of computer vision* **110**, 172–184 (2014).

- [12] Berns, R., Taplin, L., and Nezamabadi, M., “Modifications of a sinarback 54 digital camera for spectral and high-accuracy colorimetric imaging: simulations and experiments,” (2004).
- [13] Ohsawa, K., Ajito, T., Komiya, Y., Fukuda, H., Haneishi, H., Yamaguchi, M., and Ohya, N., “Six band hdtv camera system for spectrum-based color reproduction,” *Journal of Imaging Science*

- and Technology **48**(2), 85–92 (2004).
- [14] Miao, L. and Qi, H., “The design and evaluation of a generic method for generating mosaicked multispectral filter arrays,” *IEEE Transactions on Image Processing* **15**(9), 2780–2791 (2006).
- [15] Baone, G. A. and Qi, H., “Demosaicking methods for multispectral cameras using mosaic focal plane array technology,” in [*Spectral Imaging: Eighth International Symposium on Multispectral Color Science*], **6062**, 75–87, SPIE (2006).
- [16] Monno, Y., Tanaka, M., and Okutomi, M., “Multispectral demosaicking using adaptive kernel upsampling,” in [*2011 18th IEEE International Conference on Image Processing*], 3157–3160, IEEE (2011).
- [17] Monno, Y., Tanaka, M., and Okutomi, M., “Multispectral demosaicking using guided filter,” in [*Digital Photography VIII*], **8299**, 204–210, SPIE (2012).
- [18] Wang, X., Thomas, J.-B., Hardeberg, J. Y., and Gouton, P., “Median filtering in multispectral filter array demosaicking,” in [*Digital Photography IX*], **8660**, 103–112, SPIE (2013).
- [19] Monno, Y., Kiku, D., Kikuchi, S., Tanaka, M., and Okutomi, M., “Multispectral demosaicking with novel guide image generation and residual interpolation,” in [*2014 IEEE International Conference on Image Processing (ICIP)*], 645–649, IEEE (2014).
- [20] Monno, Y., Kikuchi, S., Tanaka, M., and Okutomi, M., “A practical one-shot multispectral imaging system using a single image sensor,” *IEEE Transactions on Image Processing* **24**(10), 3048–3059 (2015).
- [21] Rush, A. and Hubel, P., “X3 sensor characteristics,” *Journal of The Society of Photographic Science and Technology of Japan* **66**(1), 57–60 (2003).
- [22] Finlayson, G. D. and Zhu, Y., “Designing color filters that make cameras more colorimetric,” *IEEE Transactions on Image Processing* **30**, 853–867 (2020).
- [23] Gong, Z., Tanaka, M., Monno, Y., and Okutomi, M., “Optimal noise-aware imaging with switchable prefilters,” in [*2022 IEEE International Conference on Image Processing (ICIP)*], 2771–2775, IEEE (2022).
- [24] Taguchi, H. and Enokido, M., “Technology of color filter materials for image sensor,” *Red* **10502**(8892), 3216 (2017).
- [25] Singh, T. and Singh, M., “Disregarding Spectral Overlap - a unified approach for Demosaicking, Compressive Sensing and Color Filter Array Design,” in [*Proc. of IEEE ICIP*], (2011).
- [26] Singh, M. and Singh, T., “Linear universal demosaicking of regular pattern color filter arrays,” in [*2012 IEEE International Conference on Acoustics, Speech and Signal Processing (ICASSP)*], 1277–1280, IEEE (2012).
- [27] Zhang, C., Li, Y., Wang, J., and Hao, P., “Universal demosaicking of color filter arrays,” *IEEE Transactions on Image Processing* **25**(11), 5173–5186 (2016).
- [28] Condat, L., “A generic variational approach for demosaicking from an arbitrary color filter array,” in [*Proc. of IEEE ICIP*], (2009).
- [29] Lukac, R. and Plataniotis, K., “Universal demosaicking for imaging pipelines with an RGB color filter array,” *Pattern Recognition* **38**(11), 2208–2212 (2005).
- [30] Grenoble, F., “Frequency selection demosaicking: A review and a look ahead,”
- [31] Kopf, J., Cohen, M. F., Lischinski, D., and Uyttendaele, M., “Joint bilateral upsampling,” *ACM Transactions on Graphics (ToG)* **26**(3), 96–es (2007).
- [32] He, K., Sun, J., and Tang, X., “Guided image filtering,” *IEEE transactions on pattern analysis and machine intelligence* **35**(6), 1397–1409 (2012).
- [33] Fairchild, M. D., “A revision of ciecam97s for practical applications,” *Color Research & Application: Endorsed by Inter-Society Color Council, The Colour Group (Great Britain), Canadian Society for Color, Color Science Association of Japan, Dutch Society for the Study of Color, The Swedish Colour Centre Foundation, Colour Society of Australia, Centre Français de la Couleur* **26**(6), 418–427 (2001).
- [34] Zhang, M. and Gunturk, B. K., “Multiresolution bilateral filtering for image denoising,” *IEEE Transactions on image processing* **17**(12), 2324–2333 (2008).
- [35] Xiao, F., Farrell, J. E., DiCarlo, J. M., and Wandell, B. A., “Preferred color spaces for white balancing,” in [*Sensors and Camera Systems for Scientific, Industrial, and Digital Photography Applications IV*], **5017**, 342–350, SPIE (2003).
- [36] Zhang, L. and Wu, X., “Color demosaicking via directional linear minimum mean square-error estimation,” *IEEE Trans. on Image Processing* **14**(12), 2167–2178 (2005).
- [37] Farrell, J. E. and Wandell, B. A., “Image systems simulation,” *Handbook of Digital Imaging* **1**, 373–400 (2015).
- [38] Stockman, A., Sharpe, L. T., and Fach, C., “The spectral sensitivity of the human short-wavelength sensitive cones derived from thresholds and color matches,” *Vision research* **39**(17), 2901–2927 (1999).

Author Biography

Tripurari Singh received his Bachelors in Computer Science from the Indian Institute of Technology, Delhi, (1993) and his PhD in Computer Science from the Johns Hopkins University (1999). Thereafter he worked in the Operations Research industry, developing stochastic optimization algorithms, before switching to image processing. His work has focused on CFA design and the processing of raw sensor data in the presence of white/clear pixels, infrared pixels, chromatic aberration, multiple rounds of pixel binning and high chrominance resolution.

Mritunjay Singh has a background in Physics from Indian Institute of Technology, Mumbai and Caltech. Thereafter he worked in the Operations Research industry, developing stochastic optimization algorithms, before switching to image processing. His work has focused on CFA design and the processing of raw sensor data in the presence of white/clear pixels, infrared pixels, chromatic aberration, multiple rounds of pixel binning and high chrominance resolution.